Research Square

Preprints are preliminary reports that have not undergone peer review.
They should not be considered conclusive, used to inform clinical practice,
or referenced by the media as validated information.

Hemispheric Geomagnetic Activity Dependence on IMF By: Evidence from the Satellite and Pre-Satellite Eras

Jouni Takalo

jojuta@gmail.com

Independent researcher

Research Article

Keywords: Interplanetary Magnetic field, IMF \((B_y)\), Geomagnetic Activity, Sector Polarity, Hemispheric Asymmetry

Posted Date: November 3rd, 2026

DOI: https://doi.org/10.21203/rs.3.rs-11360911/v1

License: This work is licensed under a Creative Commons Attribution 4.0 International License.
Read Full License

Additional Declarations: No competing interests reported.

Hemispheric Geomagnetic Activity Dependence on IMF B_y: Evidence from the Satellite and Pre-Satellite Eras

Jouni Takalo[1*]

[1*]Docent, Ph.D., Independent researcher, Taivalkuja 12 B, Oulu, 90910, Finland.

Corresponding author(s). E-mail(s): jojuta@gmail.com;

Abstract

The sign of the interplanetary magnetic field (IMF) $\boldsymbol{B_y}$ is known to produce hemispheric asymmetries in the coupled magnetosphere–ionosphere system, but its long-term signature in hemispheric geomagnetic activity is less well established. We investigate whether IMF polarity organizes the distribution of geomagnetic activity between the Northern and Southern Hemispheres independently of the overall activity level. Homogeneous hemispheric $\boldsymbol{aa}$ indices are analyzed using directly measured IMF $\boldsymbol{B_y}$ during 1965–2010 and reconstructed IMF sector polarity extending back to 1868. Positive- and negative-$\boldsymbol{B_y}$ days are first compared after matching them within 5-nT bins of overall geomagnetic activity. As an independent control, the $\boldsymbol{B_y}$ dependence is estimated while accounting directly for southward IMF, solar-wind speed, and long-term variations.

A systematic $\boldsymbol{B_y}$-dependent hemispheric asymmetry remains under both control approaches, with the most consistent positive differences between $\boldsymbol{B_y > 0}$ and $\boldsymbol{B_y < 0}$ conditions occurring in May, June, and October. The seasonal organization of this hemispheric effect differs markedly from the corresponding $\boldsymbol{B_y}$ dependence of overall geomagnetic activity. The latter is dominated by an annual component with a spring–autumn reversal, whereas the activity-matched hemispheric contrast is dominated by a semiannual component with fitted maxima near May and November. Thus, the hemispheric dependence is not simply a scaled representation of the polarity-dependent seasonal modulation of total geomagnetic activity.

Reconstructed IMF sector polarity shows that the principal seasonal features of the activity-matched hemispheric contrast were already present during 1868–1964 and recur in the satellite-era reconstruction. The results suggest that IMF

$\boldsymbol{B_y}$ provides a persistent organization of the hemispheric distribution of geomagnetic activity, superposed on the better-known polarity-dependent modulation of overall geomagnetic activity.

Keywords: Interplanetary Magnetic field, IMF $\boldsymbol{B_y}$, Geomagnetic Activity, Sector Polarity, Hemispheric Asymmetry

1 Introduction

The interaction of the solar wind with the terrestrial magnetosphere is strongly controlled by the orientation of the interplanetary magnetic field (IMF). Magnetic reconnection provides the fundamental mechanism for transferring solar-wind energy and momentum into the magnetosphere [1], while the efficiency of this coupling depends on both the magnitude and orientation of the IMF [2, 3]. An important consequence is the well-known seasonal variation of geomagnetic activity. In the Russell–McPherron mechanism, the transformation of the IMF into geomagnetic coordinates produces a seasonally varying southward component whose sign and magnitude depend on the IMF sector polarity [2]. Long geomagnetic records have shown, however, that the observed seasonal variation cannot be attributed to a single mechanism. The axial and equinoctial mechanisms also contribute to its seasonal organization [4–7].

The sign of IMF B_y has long been known to modify the morphology of high-latitude convection and magnetic perturbations, with the response depending on season and dipole orientation [8, 9]. Satellite observations have subsequently demonstrated a season-dependent hemispheric asymmetry of the auroral electrojets, with the relative Northern- and Southern-Hemisphere response changing with the sign of IMF B_y [10]. The east–west IMF component, B_y, also produces systematic asymmetries in the magnetosphere and ionosphere that cannot in general be described solely in terms of the magnitude of conventional solar-wind coupling functions. IMF B_y affects magnetospheric convection, field-aligned currents, magnetic-field geometry, and the mapping between the magnetosphere and the two ionospheres [11–14]. An explicit dependence of high-latitude geomagnetic activity on the sign of IMF B_y has been demonstrated even after accounting for the usual solar-wind driving parameters [15]. Subsequent studies have found related B_y-dependent signatures in subauroral geomagnetic activity, energetic-particle precipitation, and ionospheric electrodynamics [16–20]. Recent multi-instrument observations further indicate that these asymmetries develop on characteristic magnetospheric time scales, supporting an internal magnetospheric contribution to the explicit B_y effect [21].

A north–south asymmetry associated with IMF sector polarity and B_y has, in fact, been recognized for several decades. Early geomagnetic studies reported differences between the Northern and Southern Hemispheres related to the IMF sector structure [22, 23], and [24] explicitly examined the effect of IMF B_y on the north–south asymmetry of geomagnetic activity. More recent work has provided a physical basis for such effects. IMF B_y can induce asymmetric magnetic stresses, convection patterns,

and currents in the two hemispheres [11, 13, 25]. Pitkänen et al. [25] found an IMF-B_y-dependent interhemispheric asymmetry in magnetotail plasma-sheet convection, indicating that the B_y influence extends from the ionosphere into the magnetospheric transport of magnetic flux. The response may also depend on magnetic local time, season, and dipole tilt [12, 14]. Most recently, Holappa et al. [26] showed with global MHD simulations that the combination of IMF B_y and dipole tilt can produce pronounced dawn–dusk and interhemispheric asymmetries in Kelvin–Helmholtz wave activity and reconnection geometry. Thus, several distinct magnetospheric processes provide plausible pathways through which the sign of IMF B_y can affect the partitioning of solar-wind-driven activity between the two hemispheres.

An important difficulty in identifying such a hemispheric effect from geomagnetic indices is that IMF polarity is itself associated with systematic seasonal and longer-term variations. Consequently, a difference between Northern- and Southern-Hemisphere activity observed for opposite IMF polarities does not by itself demonstrate a polarity-dependent redistribution of geomagnetic activity between the hemispheres. The problem is particularly relevant for long-term studies, for which direct solar-wind measurements are available only during the space age. The homogenized *aa* record provides corrected Northern- and Southern-Hemisphere geomagnetic indices extending back to 1868 [27, 28]. Conversely, the characteristic geomagnetic signatures of IMF sector polarity provide a means of reconstructing the sector structure before direct IMF observations [29–31]. Long-term variations in sector-polarity occurrence are also related to the heliographic-latitude dependence of the dominant IMF polarity [32]. More recent reconstructions based on geomagnetic observations from multiple observatories have extended daily IMF-polarity estimates back into the nineteenth century [33–36]. These complementary long-term records make it possible to investigate whether a hemispheric polarity effect is a persistent feature of solar-wind–magnetosphere coupling rather than a peculiarity of the satellite era.

In this study, we examine whether IMF polarity organizes the hemispheric distribution of geomagnetic activity independently of the overall activity level. We first use directly measured IMF B_y during 1965–2010 and compare the Northern- and Southern-Hemisphere homogeneous *aa* indices after matching positive- and negative-B_y days at similar levels of overall geomagnetic activity. As an independent control, we estimate the B_y dependence while accounting directly for southward IMF and solar-wind speed. We then compare the seasonal organization of the hemispheric B_y effect with the corresponding seasonal variation of overall geomagnetic activity. Finally, reconstructed IMF polarity is combined with the homogeneous hemispheric *aa* record to test whether the same basic seasonal organization can be identified before direct IMF observations became available.

2 Data and Methods

2.1 Geomagnetic activity data

Hemispheric geomagnetic activity was characterized using the homogenized *aa* index of Lockwood et al. [27, 28]. Daily values of the homogenized Northern- and Southern-Hemisphere indices, aa_{HN} and aa_{HS}, were used together with their hemispheric

mean,

$$Aa_H = \frac{Aa_{HN} + Aa_{HS}}{2}. \tag{1}$$

The homogenized *aa* record covers 1868–2017 and was used both for the satellite-era analysis and for the historical analysis based on reconstructed IMF polarity.

The normalized hemispheric asymmetry was defined as

$$A = \frac{Aa_{HN} - Aa_{HS}}{Aa_{HN} + Aa_{HS}}, \tag{2}$$

so that $A > 0$ denotes relatively stronger geomagnetic activity in the Northern Hemisphere and $A < 0$ relatively stronger activity in the Southern Hemisphere. In addition, the absolute hemispheric difference was defined as

$$D = Aa_{HN} - Aa_{HS}. \tag{3}$$

The normalized quantity A characterizes the hemispheric partitioning of geomagnetic activity relative to its overall level, whereas D expresses the corresponding difference in nT.

2.2 Direct IMF and solar-wind data

Hourly interplanetary magnetic field and solar-wind measurements were used for the satellite-era analysis covering 1965–2010. The principal IMF quantity was the GSE B_y component. GSM B_z and solar-wind speed V were additionally used to control for variations in upstream solar-wind driving.

For the activity-matched analysis, daily IMF B_y polarity was determined from the hourly measurements. A day was retained when at least 12 valid, nonzero hourly B_y measurements were available and at least 75% of these measurements had the same sign. Days satisfying these criteria were classified as either $B_y > 0$ or $B_y < 0$. Zero-valued B_y measurements were excluded from both the hourly data-coverage count and the determination of the dominant sign.

For the upstream-control analysis, the southward IMF component was defined hourly as

$$B_s = \max(-B_z, 0), \tag{4}$$

where B_z is in GSM coordinates. Daily values of B_s and solar-wind speed V were then formed from the available hourly observations. The upstream-control sample was restricted to days containing at least 12 valid hourly measurements of B_y, B_z, and V.

2.3 Activity-matched comparison of IMF B_y signs

A direct comparison of geomagnetic activity between $B_y > 0$ and $B_y < 0$ days can be affected by differences in the overall level of geomagnetic activity between the two groups. To compare the hemispheric distribution of activity at similar total activity levels, an activity-matching procedure was therefore applied separately within each calendar month.

Daily observations were divided into 5-nT bins according to Aa_H. Only activity bins containing observations from both B_y classes were retained. Within each common activity bin, the mean values of A and D were calculated separately for $B_y > 0$ and $B_y < 0$ days. The within-bin differences were then combined using the harmonic overlap weight

$$w_j = \frac{2n_{+,j}n_{-,j}}{n_{+,j} + n_{-,j}}, \tag{5}$$

where $n_{+,j}$ and $n_{-,j}$ are the numbers of $B_y > 0$ and $B_y < 0$ observations in activity bin j.

The monthly activity-matched difference in hemispheric asymmetry was consequently calculated as

$$\Delta A = \frac{\sum_j w_j \left(\overline{A}_{+,j} - \overline{A}_{-,j}\right)}{\sum_j w_j}. \tag{6}$$

The corresponding activity-matched difference in the absolute hemispheric activity was calculated analogously as

$$\Delta D = \frac{\sum_j w_j \left(\overline{D}_{+,j} - \overline{D}_{-,j}\right)}{\sum_j w_j}. \tag{7}$$

The residual difference in Aa_H was calculated as a diagnostic of the effectiveness of the activity matching.

For comparison with the hemispheric effect, the monthly difference in overall geomagnetic activity,

$$\Delta Aa_H = Aa_H(B_y > 0) - Aa_H(B_y < 0), \tag{8}$$

was also calculated without activity matching. This quantity was used to characterize the seasonal B_y dependence of the overall level of geomagnetic activity.

2.4 Control for upstream solar-wind conditions

As an alternative to conditioning on the geomagnetic response Aa_H, the B_y dependence was also estimated while controlling directly for upstream solar-wind conditions. Separate regression models were fitted for each calendar month.

For an outcome Y, representing either A or D, the model can be written schematically as

$$Y = \beta_0 + \beta_{By} I(B_y > 0) + \beta_1 B_s + \beta_2 B_s^2 + \beta_3 V + \beta_4 V^2 + \gamma_{\text{year}} + \epsilon, \tag{9}$$

where $I(B_y > 0)$ is an indicator for positive IMF B_y and γ_{year} represents year fixed effects. The coefficient β_{By} therefore estimates the adjusted difference between $B_y > 0$ and $B_y < 0$ conditions after accounting for nonlinear variations in B_s and solar-wind speed.

Standard errors were clustered in consecutive 27-day intervals to account for serial dependence on approximately solar-rotation time scales. Statistical tests were performed separately for the 12 calendar months, and the resulting p-values were adjusted

for multiple testing using the Benjamini–Hochberg false-discovery-rate procedure (FDR) [37].

2.5 Reconstructed IMF polarity

For the historical analysis, we used the reconstructed daily IMF-sector polarity data developed from ground-based geomagnetic observations by Vokhmyanin and Ponyavin [33–35] and subsequently compiled into the long-term polarity data set of Vokhmyanin and Zolotova [36]. The reconstruction exploits polarity-dependent geomagnetic variations to infer IMF sector polarity before direct spacecraft measurements became available.

The data set of Vokhmyanin and Zolotova [36] provides seven partly overlapping polarity reconstructions (C1–C7), formed from different combinations of geomagnetic observatory records. Each reconstruction provides a signed polarity parameter C, whose sign indicates the inferred IMF sector polarity and whose absolute magnitude reflects the reliability of the polarity assignment. Positive C corresponds to Away polarity and negative C to Toward polarity. As an additional validation for the present analysis, we compared the reconstructed polarity signs with directly measured daily IMF B_y during their common satellite-era coverage. The agreement increased with $|C|$ and exceeded 93% for all seven reconstructions when $|C| \geq 0.5$. We therefore retained values with $|C| \geq 0.5$ for the historical analysis. The seven reconstructions were analyzed separately, and their median was used only as a descriptive summary rather than as an independent statistical estimate.

2.6 Historical activity-matched analysis

The reconstructed IMF-polarity series were combined by date with the homogenized hemispheric aa record. For each of C1–C7, positive and negative reconstructed polarities were interpreted as Away and Toward sectors, respectively.

The historical analysis used the same 5-nT Aa_H activity-matching procedure as the direct-B_y analysis. Within each calendar month and activity bin, mean A and D were calculated separately for Away and Toward days. Only bins represented by both polarities were retained, and the binwise contrasts were combined using the harmonic overlap weighting defined above.

The resulting quantities were

$$\Delta A = A_{\mathrm{Away}} - A_{\mathrm{Toward}} \tag{10}$$

and

$$\Delta D = D_{\mathrm{Away}} - D_{\mathrm{Toward}}. \tag{11}$$

To examine the temporal persistence of the effect, the analysis was performed separately for 1868–1964 and 1965–2010. Each C series was analyzed individually. Median values across C1–C7 were used only as descriptive summaries and not as statistically independent combined estimates.

2.7 Block-bootstrap uncertainty estimation

Confidence intervals for the activity-matched monthly contrasts obtained from directly measured IMF B_y were estimated using a block bootstrap designed to retain short-term temporal dependence. The daily records were divided into consecutive 27-day calendar blocks, approximately corresponding to one solar rotation. Complete blocks were sampled with replacement, and the monthly activity-matched contrasts were recalculated from the resampled data.

A total of 5,000 bootstrap realizations were generated. The 2.5th and 97.5th percentiles of the resulting distributions were used as the limits of the 95% confidence intervals.

2.8 Annual and semiannual harmonic analysis

The seasonal organization of the monthly contrasts was quantified by fitting annual and semiannual harmonic components. For a monthly quantity $y(m)$, where $m = 1, \ldots, 12$, the fitted model was

$$y(m) = c + a_1 \cos\left(\frac{2\pi m}{12}\right) + b_1 \sin\left(\frac{2\pi m}{12}\right) + a_2 \cos\left(\frac{4\pi m}{12}\right) + b_2 \sin\left(\frac{4\pi m}{12}\right). \tag{12}$$

The annual and semiannual amplitudes were calculated as

$$R_1 = \sqrt{a_1^2 + b_1^2}, \qquad R_2 = \sqrt{a_2^2 + b_2^2}, \tag{13}$$

respectively. Thus, R_1 quantifies the strength of the once-per-year variation and R_2 the strength of the twice-per-year variation. The corresponding phases were obtained from the sine and cosine coefficients and converted to the calendar-month positions of the harmonic maxima. The annual component has one maximum and one minimum per year, separated by six months, whereas the semiannual component has two maxima per year, also separated by six months.

The harmonic decomposition was applied to the unmatched $\Delta A a_H$ and activity-matched ΔA obtained from directly measured IMF B_y.

3 Results

3.1 Dependence of hemispheric asymmetry on the sign of IMF B_y

Using directly measured IMF B_y during 1965–2010, we compared the normalized and absolute hemispheric differences, A and D [Eqs. (2) and (3)], between $B_y > 0$ and $B_y < 0$ conditions after matching the two classes by overall geomagnetic activity, as described in Section 2.3.

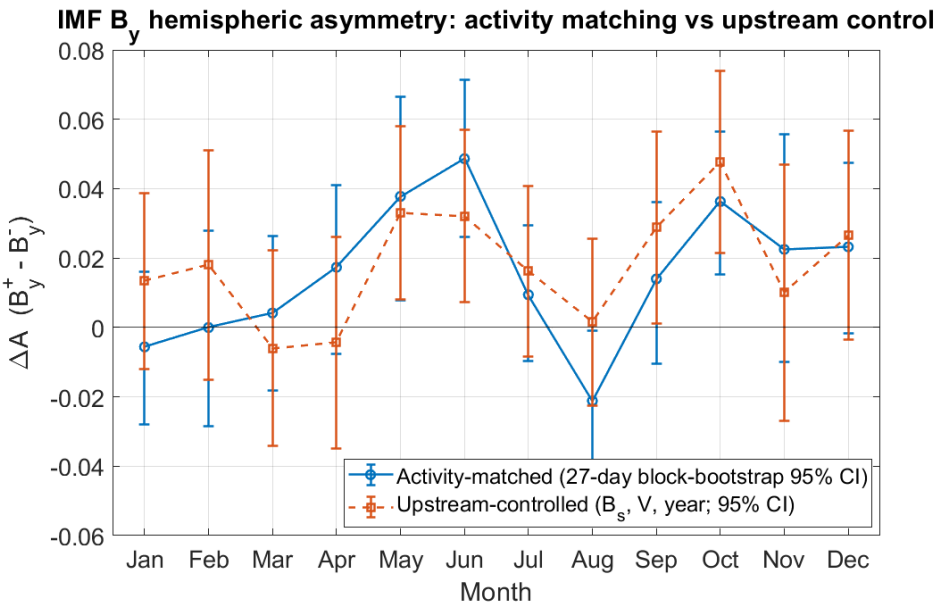


Fig. 1 Monthly IMF $B_y > 0 - B_y < 0$ difference in normalized hemispheric geomagnetic asymmetry A. Activity-matched estimates were obtained after matching $B_y > 0$ and $B_y < 0$ days within 5-nT Aa_H bins; error bars show 95% confidence intervals obtained by 27-day block bootstrap. Upstream-controlled estimates were obtained from monthly regression models controlling for B_s, solar-wind speed V, and year; error bars show 95% confidence intervals based on standard errors clustered in 27-day intervals.

The resulting B_y dependence showed a pronounced seasonal structure. Positive differences between $B_y > 0$ and $B_y < 0$ conditions occurred predominantly during April–June and September–December. The largest normalized differences were observed in June ($\Delta A = 0.0487$, 95% block-bootstrap CI 0.0266–0.0695), May ($\Delta A = 0.0373$, 0.0120–0.0631), and October ($\Delta A = 0.0363$, 0.0185–0.0534). In terms of the absolute hemispheric difference, the corresponding effects reached 1.76 nT (95% block-bootstrap CI 0.93–2.45 nT) in June and 1.97 nT (1.25–2.57 nT) in October. The seasonal structure of the directly measured B_y dependence motivated the subsequent comparison with the reconstructed IMF-polarity record.

3.2 Control for upstream solar-wind conditions

A further analysis was performed to determine whether the B_y-dependent hemispheric differences could be explained by concurrent differences in solar-wind geoeffectiveness. Rather than conditioning on the geomagnetic response Aa_H, this analysis controlled directly for upstream solar-wind parameters. Daily values of the southward IMF component,

$$B_s = \max(-B_z, 0),$$

were calculated from hourly GSM B_z, together with daily solar-wind speed V. The upstream-control analysis required at least 12 valid hourly measurements of B_y, B_z, and V, yielding 8,876 classified days during 1965–2010.

Monthly regression models included the sign of B_y, nonlinear terms for B_s and V, and year effects. Statistical uncertainties were calculated using standard errors clustered in 27-day intervals to account for serial dependence on approximately solar-rotation time scales. Probability values were subsequently adjusted across the 12 calendar months using the Benjamini–Hochberg false-discovery-rate procedure.

The B_y dependence did not disappear after controlling for B_s and V. For normalized hemispheric asymmetry, significant positive $B_y > 0 - B_y < 0$ differences remained in May ($\Delta A = 0.0330$, FDR-adjusted $q = 0.044$), June ($\Delta A = 0.0321$, $q = 0.044$), and October ($\Delta A = 0.0477$, $q = 0.0045$).

The two complementary control approaches produced positive $B_y > 0 - B_y < 0$ hemispheric asymmetry contrasts in May, June, and October. Using the activity-matched classification described in Section 2.2, the May contrast was $\Delta A = 0.0373$ (95% block-bootstrap CI 0.0120–0.0631), compared with 0.0330 (95% CI 0.0080–0.0580) after upstream control. The corresponding activity-matched and upstream-controlled estimates were 0.0487 (0.0266–0.0695) and 0.0321 (0.0074–0.0569) in June, and 0.0363 (0.0185–0.0534) and 0.0477 (0.0214–0.0739) in October. Thus, the principal seasonal B_y-dependent hemispheric asymmetry remained positive under both geomagnetic-activity matching and upstream solar-wind control.

A similar result was obtained for the absolute hemispheric difference D. The strongest and most consistent effect occurred in October, for which the activity-matched difference was $\Delta D = 1.97$ nT (95% block-bootstrap CI 1.25–2.57 nT), while the upstream-controlled estimate was 2.65 nT (95% CI 1.24–4.07 nT; $p = 2.4 \times 10^{-4}$, $q = 0.0028$). Significant upstream-controlled positive differences were also obtained in May ($\Delta D = 1.65$ nT, $q = 0.049$) and December ($\Delta D = 1.57$ nT, $q = 0.025$), while June was marginal after FDR correction ($\Delta D = 1.25$ nT, $q = 0.054$). These results indicate that the observed B_y dependence cannot be explained entirely by differences in the overall level of geomagnetic activity or by concurrent southward IMF and solar-wind speed.

3.3 Seasonal organization of the B_y-dependent hemispheric asymmetry

The seasonal variation of the hemispheric B_y effect was compared with the corresponding B_y-dependent variation in the overall level of geomagnetic activity. For this purpose, the monthly difference in Aa_H between $B_y > 0$ and $B_y < 0$ days was first calculated without activity matching. This difference showed a pronounced annual variation, with negative values during spring and positive values during autumn. In contrast, the activity-matched hemispheric difference ΔA showed positive maxima during May–June and again during autumn, with a minimum during late summer (Fig. 3).

The difference between these seasonal patterns was quantified using the annual–semiannual harmonic decomposition defined in Eq. (12). For the unmatched ΔAa_H, the annual amplitude was $R_1 = 10.82$ nT and the semiannual amplitude was $R_2 = 1.04$

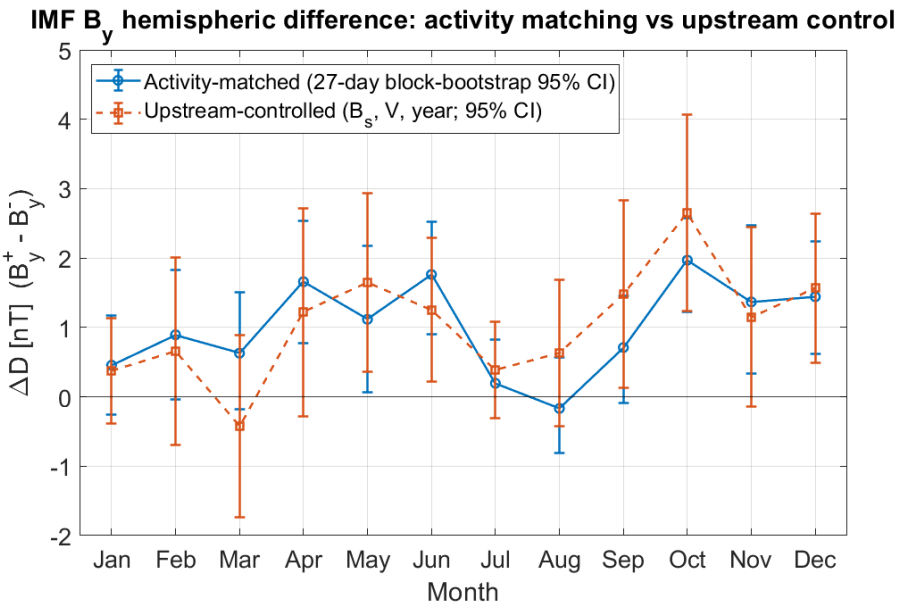


Fig. 2 As in Figure 1, but for the absolute hemispheric difference $D = Aa_{HN} - Aa_{HS}$, in nT.

nT ($R_2/R_1 = 0.096$), indicating a predominantly annual variation. In contrast, the activity-matched ΔA was dominated by the semiannual component ($R_1 = 0.0054$, $R_2 = 0.0221$; $R_2/R_1 = 4.09$), with fitted maxima near May and November.

Thus, the hemispheric B_y dependence is not simply a scaled representation of the B_y-dependent seasonal modulation of overall geomagnetic activity. The latter was predominantly annual, with a spring–autumn reversal, whereas the activity-matched hemispheric contrast was predominantly semiannual.

3.4 Persistence of the hemispheric polarity effect before the satellite era

The reconstructed IMF-polarity data were used to examine whether the hemispheric polarity dependence identified from direct IMF measurements was also present before the satellite era. The analysis was performed separately for 1868–1964 and 1965–2010 using the same 5-nT activity-matching procedure. The individual polarity reconstructions were analyzed separately, and their monthly median was used as a descriptive summary (Fig. 4).

The main seasonal structure of the activity-matched hemispheric polarity effect was already present during 1868–1964. Positive Away–Toward differences occurred in May–June and increased again during autumn, reaching their largest values toward the end of the year. Negative values occurred in July–August. The corresponding 1965–2010 reconstruction showed a similar overall pattern, with positive values in May–June and

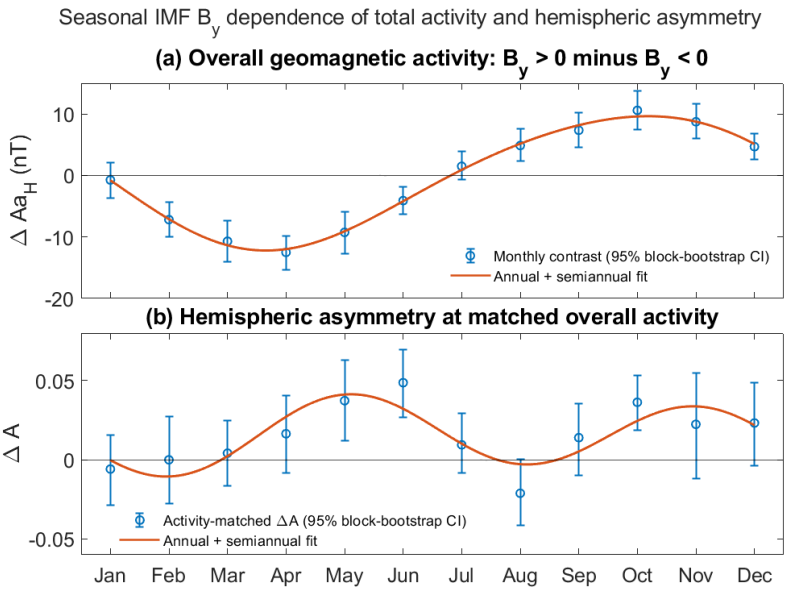


Fig. 3 Seasonal dependence of overall geomagnetic activity and hemispheric asymmetry on the sign of IMF B_y during 1965–2010. (a) Monthly difference in overall geomagnetic activity, $\Delta Aa_H = Aa_H(B_y > 0) - Aa_H(B_y < 0)$, calculated without activity matching. (b) Monthly difference in normalized hemispheric asymmetry, $\Delta A = A(B_y > 0) - A(B_y < 0)$, after matching $B_y > 0$ and $B_y < 0$ days within 5-nT Aa_H activity bins. Error bars show 95% confidence intervals obtained from 5,000 resamplings of 27-day calendar blocks. Solid curves show least-squares fits containing annual and semiannual harmonic components. The seasonal variation of the overall activity contrast is dominated by the annual component, whereas the activity-matched hemispheric contrast is dominated by the semiannual component, with fitted maxima near May and November.

October–December and a minimum in August. The individual polarity reconstructions generally reproduced these seasonal features despite their different temporal coverage.

The correspondence between the two periods was not exact. The clearest difference occurred in September, for which the median reconstructed contrast was close to zero before the satellite era but positive during 1965–2010. Nevertheless, the recurrence of the principal seasonal features in the pre-satellite record indicates that the hemispheric polarity dependence is not restricted to the era of direct IMF measurements.

4 Discussion

The results demonstrate a systematic association between the sign of IMF B_y and the hemispheric distribution of geomagnetic activity. The principal B_y-dependent differences remain when positive- and negative-B_y days are compared at similar levels of overall geomagnetic activity and also when southward IMF and solar-wind speed are controlled directly. These two approaches address different potential sources of bias. Activity matching conditions on the observed geomagnetic response, whereas the regression analysis conditions on upstream solar-wind driving. Their agreement, particularly in May, June, and October, therefore indicates that the observed hemispheric

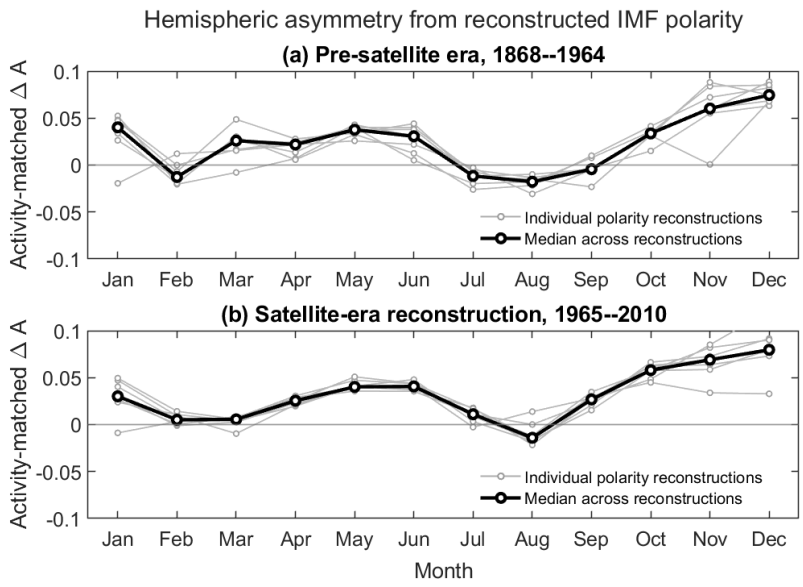


Fig. 4 Monthly activity-matched hemispheric asymmetry derived from reconstructed IMF polarity for (a) the pre-satellite period 1868–1964 and (b) the satellite-era period 1965–2010. The hemispheric contrast is defined as $\Delta A = A_{\mathrm{Away}} - A_{\mathrm{Toward}}$ after matching Away- and Toward-sector days within 5-nT Aa_H activity bins. Gray curves show the seven individual polarity reconstructions of Vokhmyanin and Ponyavin, and the black curve shows their monthly median. Only reconstructed polarity values with $|C| \geq 0.5$ were included. Positive ΔA denotes a relatively stronger Northern Hemisphere response for Away than for Toward polarity.

dependence cannot be explained solely by differences in the overall activity level or by concurrent differences in B_s and solar-wind speed.

A dependence of north–south geomagnetic asymmetry on IMF sector polarity or B_y has been recognized for several decades [22–24], and more recent studies have demonstrated IMF-B_y-dependent asymmetries in several parts of the coupled magnetosphere–ionosphere system [13, 15–21, 25]. The novelty of the present results is therefore not the existence of a B_y-dependent hemispheric asymmetry itself. Rather, the present analysis shows that such a signature is detectable in long-term homogeneous hemispheric geomagnetic indices after explicitly separating it from variations in the overall level of geomagnetic activity.

The seasonal organization of this effect provides an additional distinction between hemispheric partitioning and the modulation of overall geomagnetic activity. The unmatched $B_y > 0 - B_y < 0$ difference in Aa_H was dominated by an annual harmonic, with a spring–autumn reversal and an annual maximum near October. Such a pattern is qualitatively consistent with the well-known seasonal dependence of solar-wind–magnetosphere coupling associated with IMF orientation, including the Russell–McPherron effect [2, 4–7]. In contrast, after matching the overall geomagnetic activity level, the hemispheric contrast was dominated by a semiannual component, with fitted maxima near May and November. Consequently, the seasonal

variation of the hemispheric B_y dependence is not simply a scaled representation of the B_y-dependent seasonal modulation of total geomagnetic activity.

This result should not be interpreted as showing that the Russell–McPherron mechanism is unrelated to the hemispheric asymmetry. The Russell–McPherron effect contributes to the seasonal variation of solar-wind geoeffectiveness and therefore to the geomagnetic conditions under which the hemispheric response develops. The different harmonic composition found here instead suggests that additional seasonal factors enter the distribution of geomagnetic activity between the hemispheres. Previous studies have shown that IMF-B_y effects depend on magnetic local time, season, and dipole tilt, and can involve asymmetric magnetospheric and ionospheric responses [13, 19–21, 25]. Recent MHD simulations further show that the combination of IMF B_y and dipole tilt can produce pronounced dawn–dusk and interhemispheric asymmetries in magnetospheric dynamics [26]. Such effects provide physically plausible routes by which a seasonal B_y dependence can appear in the hemispheric geomagnetic response.

The present analysis cannot determine which of these mechanisms is primarily responsible for the observed pattern. The hemispheric *aa* indices represent integrated ground magnetic activity and do not resolve magnetic local time or individual current systems. The observed seasonal dependence may therefore reflect the combined ground signature of several B_y-dependent processes. In this respect, the long-term *aa* record is complementary to more spatially and temporally resolved observations: it provides a homogeneous measure with which to test whether the hemispheric signature persists over time, but it cannot by itself identify its magnetospheric origin.

The reconstructed sector-polarity record extends this result beyond the interval of direct IMF measurements. The principal seasonal features of the activity-matched Away–Toward contrast were already present during 1868–1964 and were again obtained from the reconstructed polarity data during 1965–2010. Both periods showed positive contrasts during late spring and toward the end of the year, together with a summer minimum. The agreement is not exact; in particular, the September contrast differs between the two periods. Nevertheless, the recurrence of the main seasonal structure indicates that the hemispheric polarity dependence is not restricted to the satellite era.

The historical extension also has important limitations. Sector polarity reconstructed from geomagnetic observations is not identical to a direct measurement of IMF B_y, and the seven C1–C7 reconstructions are partly overlapping rather than statistically independent records [33–36]. Their agreement therefore cannot be interpreted as seven independent confirmations. For this reason, the reconstructions were analyzed separately and their median was used only as a descriptive summary. The high agreement between reconstructed polarity and directly measured IMF B_y during their common interval nevertheless supports their use for examining whether the same broad hemispheric organization extends into the pre-satellite era.

Taken together, the results support a distinction between two aspects of IMF-polarity-dependent geomagnetic variability. IMF orientation modulates the overall level of geomagnetic activity, but it is also associated with how that activity is distributed between the Northern and Southern Hemispheres. The latter dependence

remains after controlling either the geomagnetic activity level or major upstream driving parameters, has a seasonal organization different from that of the overall activity contrast, and is detectable in reconstructed polarity data extending back into the nineteenth century.

5 Conclusions

We have examined the dependence of hemispheric geomagnetic activity on IMF B_y using homogeneous Northern and Southern Hemisphere *aa* indices. During 1965–2010, systematic differences between $B_y > 0$ and $B_y < 0$ conditions remained after matching the overall geomagnetic activity level. The principal seasonal differences were also retained when southward IMF, solar-wind speed, and long-term variations were controlled directly. Thus, the observed hemispheric dependence cannot be explained solely by differences in the overall level of geomagnetic activity or by these major measures of upstream solar-wind driving.

The seasonal organization of the hemispheric effect differed from that of the B_y-dependent variation in total geomagnetic activity. The latter was predominantly annual, whereas the activity-matched hemispheric contrast was predominantly semiannual, with fitted maxima near May and November. This indicates that the hemispheric effect is not simply a scaled representation of the conventional seasonal modulation of overall geomagnetic activity.

Finally, reconstructed IMF-sector polarity indicates that the main seasonal features of the hemispheric dependence were already present before direct IMF observations became available. Overall, the results suggest that IMF B_y provides a persistent organization of the hemispheric distribution of geomagnetic activity, superposed on the better-known polarity-dependent modulation of overall geomagnetic activity.

6 Acknowledgments

The author acknowledges the NASA Space Physics Data Facility and the OMNIWeb service for providing the interplanetary magnetic field and solar-wind data used in this study. The author thanks Mikhail Vokhmyanin and Natalia Zolotova for making the reconstructed IMF sector-polarity data available and Mikhail Vokhmyanin for helpful clarification concerning the interpretation of the polarity reconstructions. The homogenized hemispheric *aa* indices used in this study were provided by Lockwood et al. (2018a,b).

Funding

This research received no external funding.

Conflict of Interest

The author declares no conflict of interest.

References

[1] Dungey, J.W.: Interplanetary magnetic field and the auroral zones. Physical Review Letters **6**, 47–48 (1961) https://doi.org/10.1103/PhysRevLett.6.47

[2] Russell, C.T., McPherron, R.L.: Semiannual variation of geomagnetic activity. Journal of Geophysical Research **78**, 92–108 (1973) https://doi.org/10.1029/JA078i001p00092

[3] Newell, P.T., Sotirelis, T., Liou, K., Meng, C.-I., Rich, F.J.: A nearly universal solar wind–magnetosphere coupling function inferred from 10 magnetospheric state variables. Journal of Geophysical Research: Space Physics **112**, 01206 (2007) https://doi.org/10.1029/2006JA012015

[4] Cliver, E.W., Kamide, Y., Ling, A.G.: Mountains versus valleys: Semiannual variation of geomagnetic activity. Journal of Geophysical Research: Space Physics **105**(A2), 2413–2424 (2000) https://doi.org/10.1029/1999JA900439

[5] Cliver, E.W., Kamide, Y., Ling, A.G.: The semiannual variation of geomagnetic activity: Phases and profiles for 130 years of aa data. Journal of Atmospheric and Solar-Terrestrial Physics **64**(1), 47–53 (2002) https://doi.org/10.1016/S1364-6826(01)00093-1

[6] Cliver, E.W., Svalgaard, L., Ling, A.G.: Origins of the semiannual variation of geomagnetic activity in 1954 and 1996. Annales Geophysicae **22**(1), 93–100 (2004) https://doi.org/10.5194/angeo-22-93-2004

[7] Zhao, H., Zong, Q.-G.: Seasonal and diurnal variation of geomagnetic activity: Russell–mcpherron effect during different imf polarity and/or extreme solar wind conditions. Journal of Geophysical Research: Space Physics **117**(A11), 11222 (2012) https://doi.org/10.1029/2012JA017845

[8] Friis-Christensen, E., Wilhjelm, J.: Polar cap currents for different directions of the interplanetary magnetic field in the y-z plane. Journal of Geophysical Research **80**, 1248–1260 (1975)

[9] Ruohoniemi, J.M., Greenwald, R.A.: Dependencies of high-latitude plasma convection: Consideration of interplanetary magnetic field, seasonal, and universal time factors in statistical patterns. Journal of Geophysical Research: Space Physics **110**(A9), 09204 (2005) https://doi.org/10.1029/2004JA010815

[10] Smith, A.R.A., Beggan, C.D., Macmillan, S., Whaler, K.A.: Climatology of the auroral electrojets derived from the along-track gradient of magnetic field intensity measured by pogo, magsat, champ, and swarm. Space Weather **15**(10), 1257–1269 (2017) https://doi.org/10.1002/2017SW001675

[11] Tenfjord, P., Østgaard, N., Snekvik, K., Laundal, K.M., Reistad, J.P., Haaland, S.,

Milan, S.E.: How the imf by induces a by component in the closed magnetosphere and how it leads to asymmetric currents and convection patterns in the two hemispheres. Journal of Geophysical Research: Space Physics **120**, 9368–9384 (2015) https://doi.org/10.1002/2015JA021579

[12] Laundal, K.M., Finlay, C.C., Olsen, N., Reistad, J.P.: Solar wind and seasonal influence on ionospheric currents from swarm and champ measurements. Journal of Geophysical Research: Space Physics **123**, 4402–4429 (2018) https://doi.org/10.1029/2018JA025387

[13] Workayehu, A.B., Vanhamäki, H., Aikio, A.T., Shepherd, S.G.: Effect of interplanetary magnetic field on hemispheric asymmetry in ionospheric horizontal and field-aligned currents during different seasons. Journal of Geophysical Research: Space Physics **126**, 2021–029475 (2021) https://doi.org/10.1029/2021JA029475

[14] Wang, H., Sun, Y., Lühr, H.: Interplanetary magnetic field by effects on the strength and latitude of field-aligned currents in different magnetic local time sectors. Journal of Geophysical Research: Space Physics **129**, 2023–032188 (2024) https://doi.org/10.1029/2023JA032188

[15] Holappa, L., Mursula, K.: Explicit imf by-dependence in high-latitude geomagnetic activity. Journal of Geophysical Research: Space Physics **123**, 4728–4740 (2018) https://doi.org/10.1029/2018JA025517

[16] Holappa, L., Gopalswamy, N., Mursula, K.: Explicit imf by-effect maximizes at subauroral latitudes. Journal of Geophysical Research: Space Physics (2019) https://doi.org/10.1029/2018JA026285

[17] Holappa, L., Asikainen, T., Mursula, K.: Explicit imf by-dependence in high-latitude geomagnetic activity: Relation to precipitating electrons. Geophysical Research Letters (2020) https://doi.org/10.1029/2019GL086676

[18] Holappa, L., Robinson, R.M., Pulkkinen, A., Asikainen, T., Mursula, K.: Explicit imf by-dependence in geomagnetic activity: Quantifying ionospheric electrodynamics. Journal of Geophysical Research: Space Physics **126**, 2021–029202 (2021) https://doi.org/10.1029/2021JA029202

[19] Laitinen, J., Holappa, L., Vanhamäki, H.: A combined effect of the earth's magnetic dipole tilt and imf B_y in controlling auroral electron precipitation. Journal of Geophysical Research: Space Physics **129**, 2023–032040 (2024) https://doi.org/10.1029/2023JA032040

[20] Laitinen, J., Holappa, L., Vanhamäki, H.: The polarity of imf B_y strongly modulates particle precipitation during high-speed streams. Geophysical Research Letters **51**(17), 2024–110877 (2024) https://doi.org/10.1029/2024GL110877

[21] Laitinen, J., Holappa, L., Vanhamäki, H., Milan, S.E.: Timescales of asymmetries in magnetospheric dynamics induced by the imf B_y component. Journal of Geophysical Research: Space Physics **130**(12), 2025–034401 (2025) https://doi.org/10.1029/2025JA034401

[22] Siebert, M.: Magnetic activity differences between the two hemispheres following the sector structure of the interplanetary magnetic field. Journal of Geophysical Research **73**(9), 3049–3052 (1968)

[23] Yoshizawa, K.: Influence of imf-sector polarity on the north-south asymmetry of geomagnetic activity and its relationship with solar wind parameters. Planetary and Space Science **32**(5), 605–610 (1984)

[24] Yoshizawa, K.: Effect of the imf-B_y component on the north-south asymmetry of geomagnetic activity. Planetary and Space Science **34**, 639–644 (1986) https://doi.org/10.1016/0032-0633(86)90041-3

[25] Pitkänen, T., Kullen, A., Laundal, K.M., Park, J.-S., Hamrin, M., De Spiegeleer, A., Chong, G.S., Tian, A.M.: Imf B_y influence on magnetospheric convection in earth's magnetotail plasma sheet. Geophysical Research Letters (2019) https://doi.org/10.1029/2019GL084190

[26] Holappa, L., Nykyri, K., Laitinen, J., Burkholder, B.: Imf by-controlled dawn–dusk and hemispheric asymmetries of kelvin–helmholtz waves and reconnection geometry under negative dipole tilt. Geophysical Research Letters **53**(18), 2026–124835 (2026) https://doi.org/10.1029/2026GL124835

[27] Lockwood, M., Chambodut, A., Barnard, L.A., Owens, M.J., Clarke, E., Mendel, V.: A homogeneous aa index: 1. secular variation. Journal of Space Weather and Space Climate **8**, 53 (2018) https://doi.org/10.1051/swsc/2018038

[28] Lockwood, M., Finch, I.D., Chambodut, A., Barnard, L.A., Owens, M.J., Clarke, E.: A homogeneous aa index: 2. hemispheric asymmetries and the equinoctial variation. Journal of Space Weather and Space Climate **8**, 58 (2018) https://doi.org/10.1051/swsc/2018044

[29] Svalgaard, L.: Interplanetary magnetic-sector structure, 1926–1971. Journal of Geophysical Research **77**(22), 4027–4034 (1972) https://doi.org/10.1029/JA077i022p04027

[30] Svalgaard, L.: Polar cap magnetic variations and their relationship with the interplanetary magnetic sector structure. Journal of Geophysical Research **78**(13), 2064–2078 (1973) https://doi.org/10.1029/JA078i013p02064

[31] Vennerstrøm, S., Zieger, B., Friis-Christensen, E.: An improved method of inferring interplanetary sector structure, 1905–present. Journal of Geophysical Research: Space Physics **106**(A8), 16011–16020 (2001) https://doi.org/10.1029/

2000JA000103

[32] Rosenberg, R.L., Coleman, J. P. J.: Heliographic latitude dependence of the dominant polarity of the interplanetary magnetic field. Journal of Geophysical Research **74**(24), 5611–5622 (1969) https://doi.org/10.1029/JA074i024p05611

[33] Vokhmyanin, M.V., Ponyavin, D.I.: Inferring interplanetary magnetic field polarities from geomagnetic variations. Journal of Geophysical Research **117**, 06102 (2012) https://doi.org/10.1029/2011JA017060

[34] Vokhmyanin, M.V., Ponyavin, D.I.: Sector structure of the interplanetary magnetic field in the nineteenth century. Geophysical Research Letters **40**, 3512–3516 (2013) https://doi.org/10.1002/grl.50749

[35] Vokhmyanin, M.V., Ponyavin, D.I.: Reconstruction of the sector structure of the interplanetary magnetic field by geomagnetic station data. Journal of Geophysical Research: Space Physics **121**, 11943–11952 (2016) https://doi.org/10.1002/2016JA023138

[36] Vokhmyanin, M., Zolotova, N.: Long-term north–south asymmetry of the heliospheric current sheet. The Astrophysical Journal **928**(1), 56 (2022) https://doi.org/10.3847/1538-4357/ac5630

[37] Benjamini, Y., Hochberg, Y.: Controlling the false discovery rate: A practical and powerful approach to multiple testing. Journal of the Royal Statistical Society: Series B (Methodological) **57**(1), 289–300 (1995)